Journal of Mines, Metals and Fuels, *71(12B) : 277-285; 2023. DOI: 10.18311/jmmf/2023/45624*

Print ISSN : 0022-2755

Journal of Mines, Metals and Fuels

Contents available at: *www.informaticsjournals.com/index.php/jmmf*

Microstructural Characterization and Mechanical Properties of LDSS2101 Using Gas Tungsten Arc Welding

Sravanthi Gudikandula[1], Ambuj Sharma[1*], Amit Kumar[2], B. Ratna Sunil[3] and Pushkar Jha[4]

[1]School of Mechanical Engineering, VIT-AP University, Amaravati - 522237, Andhra Pradesh, India; sharma.ambuj@vitap.ac.in

[2]Department of Mechanical Engineering, Sardar Vallabhbhai National Institute of Technology, Surat - 395007, Gujarat, India

[3]Department of Mechanical Engineering, College of Engineering, Prince Mohammad Bin Fahd University, Al Khobar 31952, Saudi Arabia

[4]School of Mechanical Engineering, KIIT Deemed to be University, Bhubaneswar - 751024, Odisha, India

Abstract

The Lean Duplex Stainless Steels (LDSS) consisting of low alloying element composition are a good alternative in comparison to the Duplex stainless steels and Austenitic stainless steels because of their low cost. These LDSSs are commonly used in nuclear and marine industries, desalination plants, and pressure vessels where enhanced mechanical and corrosion behavior are major requirements. In this paper, LDSS2101 is welded using Gas tungsten arc welding by heat input 0.85 kJ/mm in order to enhance the microstructural and mechanical properties. The influence of the heat input is studied to understand the microstructural characterization using optical microscopy and scanning electron microscope. The mechanical properties such as tensile and impact energy using fracture analysis are examined. Also, the scratch hardness is evaluated and compared with the micro-hardness to understand the performance of weldments. The effect of heat input carried on GTAW of 2101 has led to the significant microstructural evolution in the welded zone with good austenite reformation. The mechanical results of the weldment showed the enhancement in welded zone which is likely suitable for industrial applications.

Keywords: Austenitic Stainless Steel, Duplex Stainless Steel, Lean Duplex Stainless Steel, Microstructure, Scratch Hardness

1. Introduction

The properties after welding showed a good influence on the materials and be used in industrial applications. Duplex stainless steels (DSS) have become a good alternative to austenite steels (ASS) because of the good combination of mechanical properties and corrosion resistance[1,2]. These DSS have a microstructure of ferrite and austenite with balanced phase fraction[3,4]. The development and application of the DSS alloys have increased also with the new steel production techniques. These resulted in numerous industrial applications such as nuclear industries which require high thermal stability in power generation system pipelines and secure radioactive material transportation equipment, offshore oil industries, chemical process industries, and structures

**Author for correspondence*

for use in marine industries[5-9]. DSS Has good weldability, however, there is a possibility of higher ferrite formation, nitrides, and intermetallic precipitates in weld and heat-affected zone (WZ) and (HAZ)[10]. The balanced ferrite/austenite microstructure can be maintained by avoiding such precipitates[11]. In past years, the demand for SS has been rapidly increasing, however, the production cost also increased because of the high Ni prices which led to the development of new lean stainless steels[12,13]. LDSS 2101 is a lean DSS consisting of Mn, N with increased contents and Ni with reduced content[14-16]. These steels have a lean alloy content and unlike other duplex stainless steels; it consists of low contents of molybdenum. These lean alloys are developed in order to compete with the austenitic AISI 316 grade alloys, which have the yield strength twice and the resistance to SCC is significantly higher. Using over-alloyed filler metals, the weldability of the duplex stainless steel is enhanced[14]. The lower fractions of Ni help stabilize the austenite phase fraction in DSS microstructures and the Mo is used to reduce the secondary phase precipitation[17]. The LDSS 2101 with higher nitrogen levels and lower molybdenum improved the austenite reformation when compared to other duplex grades.

Few researchers have carried out work on microstructural behavior, and mechanical properties in LDSS2101 grade. The Gas Tungsten Arc Welding (GTAW) processes are preferred in the characterization of duplex stainless steels as they produce good quality welds[18-21]. Liljas *et al.* mentioned the applications of the new duplex family LDSS2101. He also mentioned that LDSS2101 can replace ASS of 304 type and few of structural steels. In addition, austenite reforms quickly from high temperatures[16]. Westin investigated the effect of alloying elemental composition and thermal analysis on phase analysis and microstructural characterization at higher temperatures in HAZ of DSS 2101[17]. Verma and Muthupandi concluded from their investigations that the equal phase ratio of ferrite and austenite showed good performance of LDSS weldments. They stated that the phase ratio depends on the heat input parameters which upon welding has a higher influence. The authors understood that the favorable balanced phase ratio is attained by the high heat input which resulted in a slow cooling rate[22,23]. Material processing methods such as friction stir processing and welding are also used to enhance the mechanical properties of the metals[24-27]. The corrosion resistance of the materials is enhanced by adding graphene as a reinforcement[28,29]. From the literature, it is understandable that an accurate welding process with appropriate welding conditions and parameters is necessary for efficient results. The main objective of research is to analyze the heat input effect on microstructural and mechanical properties of LDSS 2101 welded by using the GTAW process.

2. Material and Methodology

The specimens with the dimension of 250*100*8 mm are attained for the present work. The elemental composition of the LDSS2101 with filler wire ER2209 is noted in Table 1. Specimens are clamped in a welding table for a conventional GTAW process. Single-pass welding with a V-groove is made using ER2209 filler wire with a diameter of 3.15mm. The welding parameters for the present GTAW process are considered as current 74 A, and a voltage of 21V can be seen in Table 2. The heat input of 0.85 kJ/mm is considered to produce a good weld joint. Fig.1 shows the base sample and welded sample of LDSS2101. The microstructure of the welded specimen and its phases are noticed using optical microscopy. The specimens for microstructural investigations are grounded successively from 180-2000 grit emery papers and polished using diamond paste. The polished specimens are etched in Kallings reagent for 20-25 sec. The optical images of the WZ and HAZ are observed using optical and scanning electron microscopy. The ferrite and austenite phases are measured.

The tension test is carried out using ASTM standard E8M -04 at a strain rate of 2 mm/min at room temperature. Fractography tests are carried out to carry out to understand the fracture analysis. The impact toughness with fractography analysis is also measured to understand the toughness of the material. The microhardness test is carried out with the 10 kg load of about 10 -25 seconds on surface of the sample to evaluate the hardness variation according to ASTM E9231. The scratch analysis is evaluated to understand the effect of heat input and find the scratch performance on the weldment using the scratch tester equipment - TR-101-IAS with a Diamond Rockwell C-type indenter using ASTM standard G171. The test is carried out at a stroke length of 10mm from center to base at a scratch speed of 1 mm/sec along the longitudinal direction. A constant load of 15N is applied for both longitudinal directions for GTAW to measure the traction force and coefficient of friction in the welded

specimen. The scratch profiles are examined by optical microscopy.

3. Results and Discussion

3.1 Microstructural Behaviour

The SEM image of lean duplex grade LDSS 2101 base sample is shown in Figure 2. The microstructure is a two phase with alternative ferrite and austenite phase fraction. The typical two-phase structure of LDSS 2101 base material with proportions of almost equal ratios is measured. The ferrite (δ) is a continuous matrix embedded with an austenite phase (ϒ) which is discontinuous light-etched banded regions. The solidification mode for the present work is observed to be ferrite solidification mode with the austenite nucleating below the ferrite regions[30].

Figure 3 shows the welded zone, interference line, and the heat-affected zone microstructures obtained from the carried-out heat input of LDSS 2101. It showed that the typical microstructure of LDSS 2101 weld consists of ferrite phases (δ) with reformed austenite (ϒ). The different morphologies of the austenite phase appeared as Grain Boundary Austenite (GBA), Inter-Granular Austenite (IGA), and Widmanstatten Austenite (WA)[15,31,32] shown in Figure 4. During initial cooling stage, the (GBA) phase nucleates from ferrite grain boundaries and the Widmanstatten secondary austenite formation is seen and is e developed into ferrite grains. The intergranular austenite (IGA) formation can be seen inside the ferrite grains[33]. During welding it is essential to check the arc power is sufficient enough to provide good austenite reformation in WZ and HAZ.

Table 1. Elemental composition of LDSS2101 and ER2209 filler

Sample	Cr	C	Cu	Ni	Mo	Si	Mn	N	P
LDSS 2101	21.24	0.031	0.32	1.52	0.35	0.68	4.78	0.24	0.03
ER 2209	21.8	0.03	0.01	6.8	3.1	0.9	1.0	0.13	0.026

Table 2. Weld parameters of the present study

Sample	Current(A)	Voltage(V)	Heat input (kJ/mm)	Filler diameter (mm)	Root gap (mm)	Plate distance (mm)	Weld time (Sec)
0.85Kj/mm sample	74	21	0.85	3.15	2	100	55

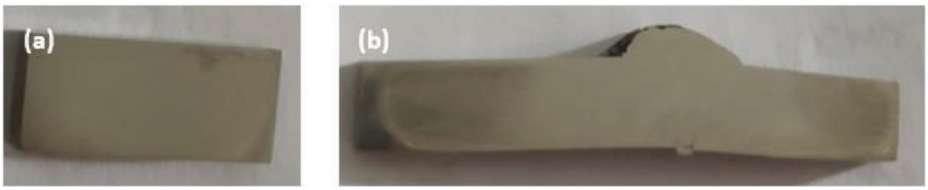


Figure 1. **(a)** Base material; **(b)** welded sample of LDSS 2101.

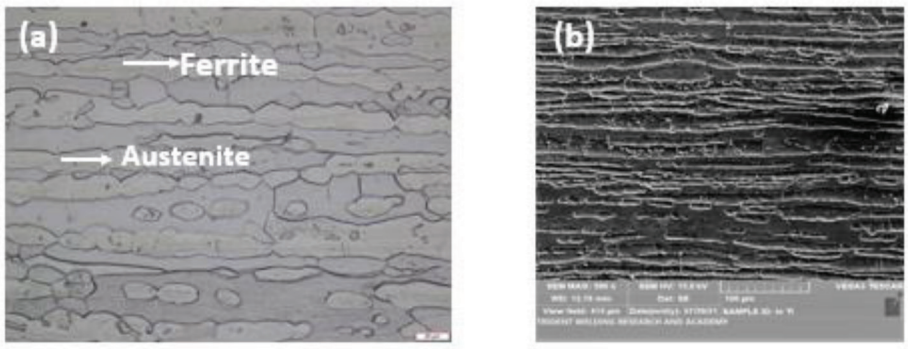


Figure 2. Optical and SEM microstructure of the base metal: **(a)** Optical microstructure **(b)** SEM microstructure.

The weldment microstructure showed a good amount of increase in austenite fraction. This phenomenon is understood by the rate of cooling which allowed the F (δ) to A (ϒ) transformation. Therefore, due to the austenite stabilizing elements, a good amount of (ϒ) austenite is transformed. The ferrite and austenite contents measured for weldment are shown in Table 3. XRD patterns of weldment and BM are shown in Figure 5. The intense peaks of ferrite and austenite can be observed in the XRD graph. The weldment specimen showed optimally proper ferrite and austenite phases with stronger (111) plane orientation. Therefore, from the XRD data, it is revealed that no intermetallic precipitates or detrimental phases are detected.

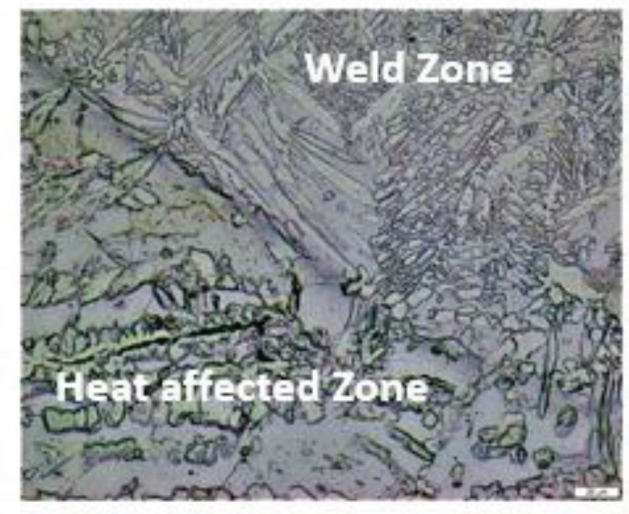


Figure 3. Welded sample with different zones.

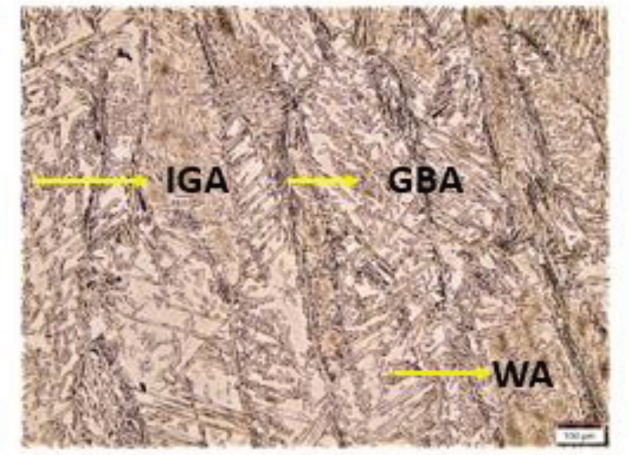


Figure 4. Different modes of austenite.

Figure 6 shows the SEM image of the weldment. Compared to the BM, it is seen that the microstructure displayed alterations in grain morphology depending on the amount of heat input carried. It is found that insufficient GBA phase development leads to the creation of additional coarse ferrite grains. It is observed that new coarse ferrite grains are formed due to insufficient GBA phase formation. The morphological characteristics of the weldment compared to the BM have changed because

Table 3. Ferrite and austenite phase fraction

Specimen	Ferrite	Austenite
weldment	55.87	44.13

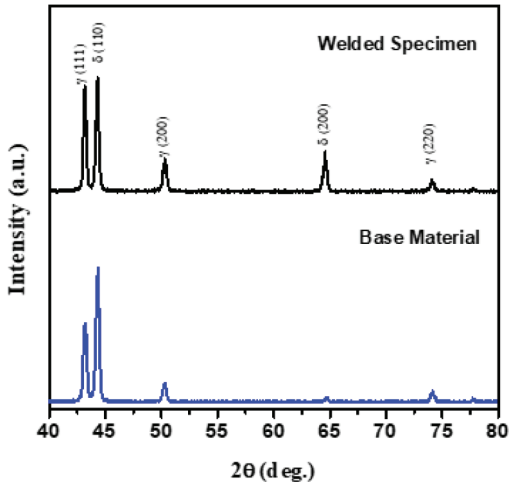


Figure 5. XRD diffraction pattern.

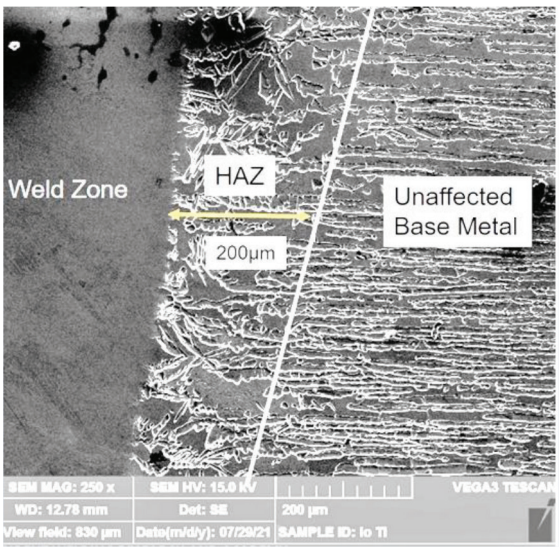


Figure 6. SEM image of HAZ.

of the parameters such as elemental composition at the weld joint and the welding parameters[22,23]. It showed that the HAZ showed a narrow extent of 200 µm which is influenced by heat input during welding. The heat inputs used during the welding process can affect grain development.

The SEM attached EDS line-scan is evaluated to observe the alloying elemental composition of WZ, HAZ and interface. Table 4. shows the major alloying elements in the WZ and HAZ of the specimen. These scans showed a good gradient of element concentration (Ni, Mn) along the fusion line between WZ and HAZ. This is due to the different elemental composition between the base material and filler wire which can be seen in Table 1. From the analysis, it is noticed that the chromium (Cr) content is varied from WZ to HAZ with respect to Mn and Ni. The filler material ER2209 is the reason for the high amounts of Ni and Mo concentrations in WZ.

Table 4. EDS alloying elements of WZ and HAZ

Specimen	zone	Cr	Ni	Mn
Base metal		21.35	2.26	6.03
Welded specimen	WM HAZ	23.93 22.04	7.46 1.67	2.20 4.97

3.2 Mechanical Properties

The tensile test is performed to illustrate the weldment strength. The weldment strength is compared with the base material is presented in Table 5. It is noticed that weldment showed good strength. The Ultimate Tensile Strength (UTS) of the weldment is 705 MPa while BM showed 680 MPa. This is due to the formation of the refined grains and the high cooling rate due to the considered heat input[3,4]. The weld strength is about 3.7 % higher than base material. The yield strength of weldment and base material are computed as 528 and 495 respectively. The Ni-based filler ER2209 increased the yield strength of the weldment which promoted the strength of the weldment. The fractography analysis is performed on tensile weldment. The necking phenomenon resulted in the plastic deformation of samples before fracture. The fracture is observed from HAZ to the weld region in the weldment specimen. The fractography picture of the tensile weldments is shown in Figure 7a. The fractography analysis showed uniform dimples on the fracture surface which resulted in ductile failure. Table 5 depicts the impact samples tested at room temperature. It is noticed that the weldment is ductile fractured after the Charpy impact test shown in Figure 7b. It is also reported that the impact toughness value of weldment is 125J and the base is 300J. The weldment has low toughness than the base material

Table 5. Tensile and impact test values

Sample	UTS(MPa)	Yield strength (MPa)	Elongation (%)	Mode of Fracture	Impact Toughness(J)
Base	680	495	28.07%	Ductile	300
weldment	705	528	25.3%	Ductile	125

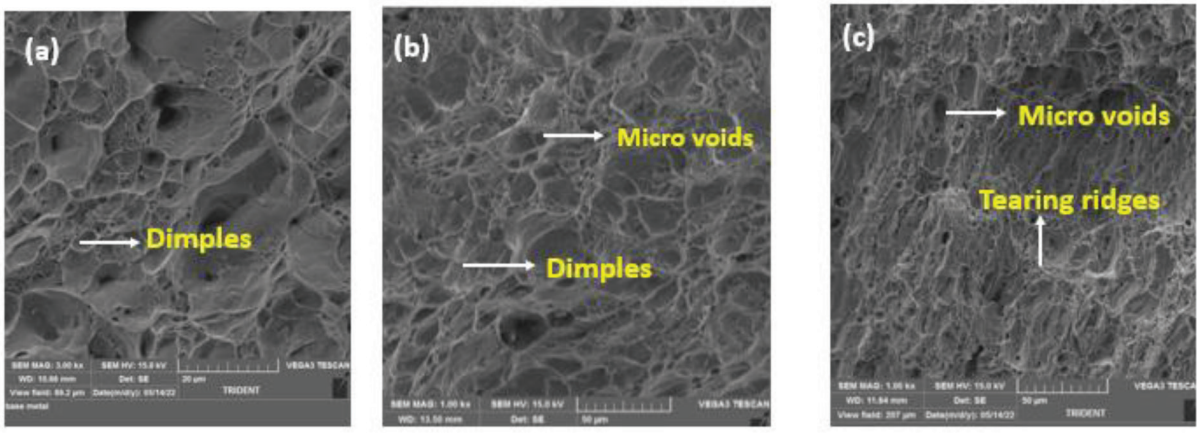


Figure 7. Fractography **(a)** tensile fractography of base material **(b)** tensile fractography of GTAW weldment and **(c)** impact test fractography of GTAW weldment.

may be due to the cooling rate. The observed impact toughness variation is due to the elemental composition and phase fraction ratio.

3.3 Microhardness Variation

The microhardness distribution on the welded specimen is carried out and is depicted in Figure 8. Results shows that, the average microhardness value of the WZ IS 252 for the heat input considered. The average hardness value of the BM is recorded as 230. The weld zone experienced higher hardness than the base material and heat-affected zone. This high microhardness is observed because of the high cooling rate due to the heat input applied which led to the grain refinement and ER2209 filler material used during welding. Also, the reduction of austenite grain size in the welded regions with respect to the BM[30]. This grain refinement can be noticed in the optical microstructure from Figures 2 and 3.

3.4 Scratch Test

In the present work, scratch analysis is evaluated on the welded sample of GTAW for 0.85kJ/mm heat input using scratch tester equipment. Both transverse and longitudinal directions are used to conduct the scratch test. Prior to the scratch analysis, the metal surface is polished. For longitudinal direction scratch analysis, the stroke length is considered 15mm from the weld center. For transverse direction, the stroke length is 5mm from weld center to base. A single pass scratch is carried out at a constant load of 15N from the weld center to the base material. Figure 9 a and b show the comparison of Traction Force (TF) and Coefficient Of Friction (COF) with stroke length in the longitudinal direction. Figure 10 a and b show the graph of TF and COF with stroke length in the transverse direction. The TF and COF are varied as there can be different damages that occur during scratching. These changes are the result of microstructural changes and surface roughness changes. Figure 11 shows the optical scratch sample. Ploughing with small debris is observed in the weldment of GTAW. Weldment of GTAW with good yield strength and high scratch hardness with good ferrite phase and refined microstructure showed good scratch resistance to the material.

Figures 9(a) and 10(a) depict the plot of traction force Vs stroke length in various zones such as weld

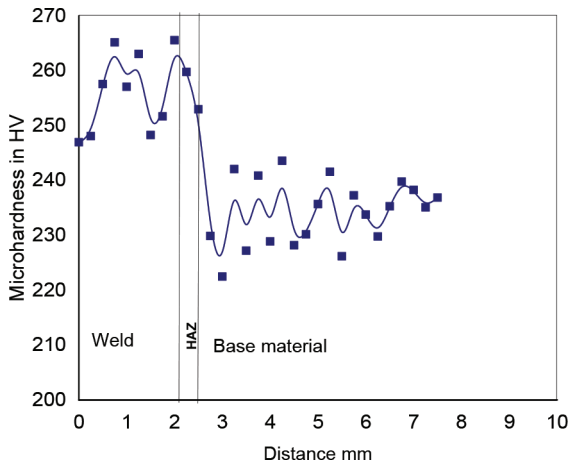
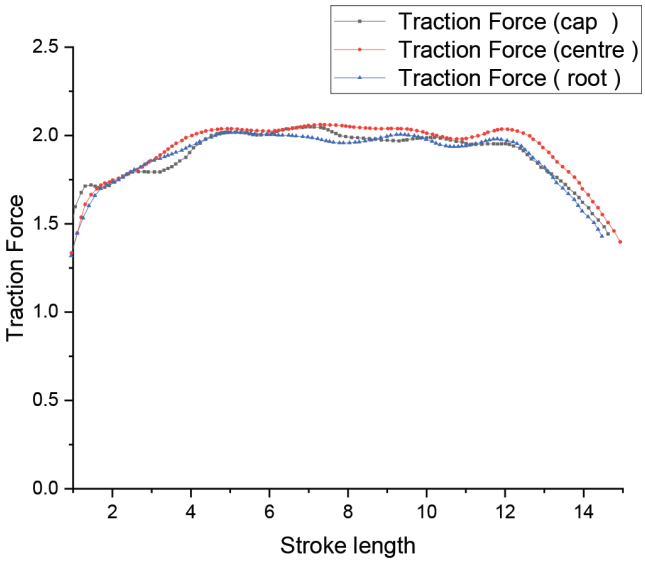
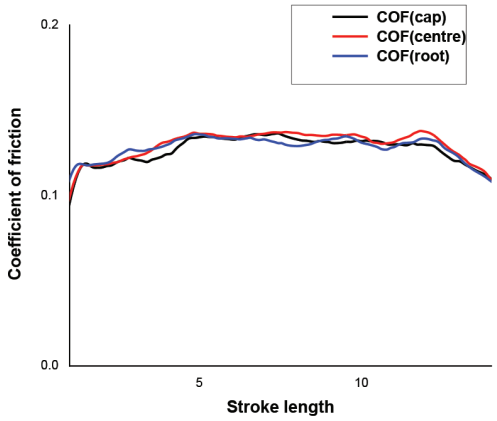


Figure 8. Microhardness plot of 2101 welded sample.



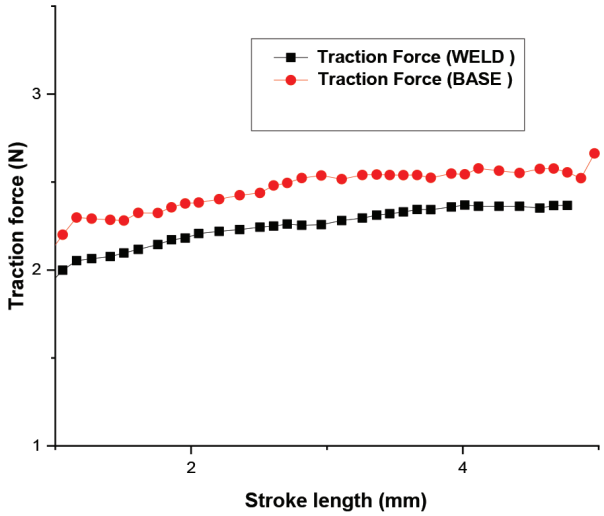
(a)



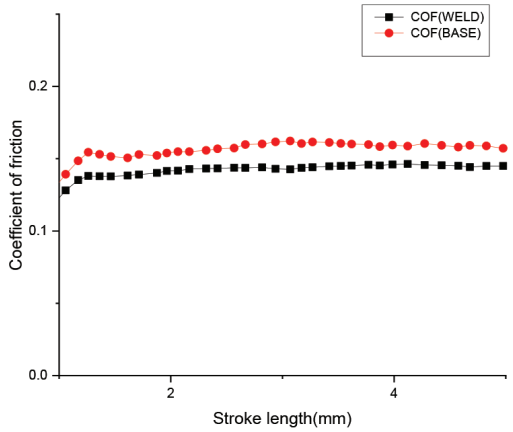
(b)

Figure 9. **(a)** Traction force of the weld sample **(b)** Coefficient of friction of the weld sample.

cap, weld center, and weld root. Figures 9(b) and 10(b) depicts the coefficient of friction vs stroke length. The results show that welded sample at the cap region showed lowest TF and CoF and also the highest TF and CoF are recorded at root region. The scratch width is less for cap regions. Scratch hardness is increased with decrement in scratch width stating that there is increment in scratch resistance. From Figure 11, weld sample showed ploughing and formation of very small debris. Good yield strength with high hardness and higher ferrite phase fraction with finer austenite levels in the microstructure of welded sample shows good scratch resistance.



(a)



(b)

Figure 10. Comparison of base material and welded samples **(a)** Traction force and **(b)** coefficient of friction.

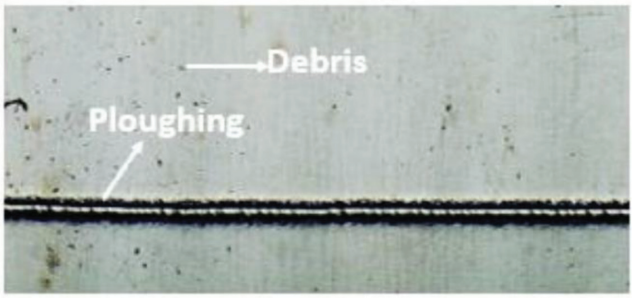


Figure 11. Optical scratch specimen.

4. Conclusion

The influence of heat input is studied on the LDS S32101. The S32101 was welded using GTA welding with electrode ER2209. The microstructural behavior of the weldment is studied using optical microscopy, scanning electron microscopy attached EDS, and XRD analysis. Microhardness and the scratch analysis of the samples are examined. From the experimental results, the following conclusions are observed:

(1) The microstructure of the welded sample at 0.85Kj/mm showed good austenite and ferrite phases with no intermetallic and secondary phase precipitates.
(2) Welded samples displaced higher ultimate tensile strength than the base material. Fractography of tensile fracture samples confirms the ductile mode of the failure of weldments.
(3) The impact weld samples are low than base material, while it exceeds the minimum threshold of 40 J required for industrial applications.
(4) From the microhardness test, the weld zone showed a higher hardness value than HAZ and base material due to the grain refinement.
(5) The scratch analysis showed that welded regions had low traction force and low COF with better scratch resistance.

5. References

1. Poznansky A, Nalbone CS, Crawford JD. The corrosion resistance of 25 Cr--3. 5 Mo--6 Ni and 25 Cr--4. 5 Mo--6 Ni cast duplex stainless steels. Duplex Stainless Steels. 1982; 431-44.
2. Honeycombe J, Gooch TG. Intergranular attack in welded stress-corrosion resistant stainless steels. Weld J. 1977; 56(11):339s-53s.

3. Gunn R. Duplex stainless steels: microstructure, properties and applications. Woodhead publishing. 1997. https://doi.org/10.1533/9781845698775
4. Paulraj P, Garg R. Effect of welding parameters on mechanical properties of GTAW of UNS S31803 and UNS S32750 weldments. Manufacturing Review. 2015; 2:29. https://doi.org/10.1051/mfreview/2015032
5. Tynell M. Applicability range for a high-strength duplex stainless steel in deep sour oil and gas wells. Journal of Materials for Energy Systems. 1983; 5(2):84-7. https://doi.org/10.1007/BF02833533
6. Miyuki H, Kudo T, Koso M, Miura M, Moroishi, T. 25%Cr containing duplex phase stainless steel for hot seawater applications. Proc. Conf. Duplex Stainless Steels.1983; 95-112.
7. Alvarez-Armas I. Duplex stainless steels: a brief hitory and some recent alloys. Recent Patents on Mechanical Engineering. 2008; 1(1):51-7. https://doi.org/10.2174/2212797610801010051
8. Fujii K, Fukuya K. Effects of radiation on spinodal decomposition of ferrite in duplex stainless steel. Journal of Nuclear Materials. 2013; 440(1-3):612-6. https://doi.org/10.1016/j.jnucmat.2013.04.072
9. Betini EG, Gomes MP, Milagre MX, Machado CD, dos Reis LA, Mucsi CS, Orlando MT, Luz TS, Martinez LG, Rossi JL. Study on welding thermal cycle and residual stress of UNS S32304 duplex stainless steel selected as external shield for a transport packaging of Mo-99. Brazilian Journal of Radiation Sciences. 2019; 7(2A (Suppl.)). https://doi.org/10.15392/bjrs.v7i2A.679
10. Hosseini VA, Wessman S, Hurtig K, Karlsson L. Nitrogen loss and effects on microstructure in multipass TIG welding of a super duplex stainless steel. Materials and Design. 2016; 98:88-97. https://doi.org/10.1016/j.matdes.2016.03.011
11. Valiente Bermejo MA, Karlsson L, Svensson LE, Hurtig K, Rasmuson H, Frodigh M, Bengtsson P. Effect of shielding gas on welding performance and properties of duplex and super duplex stainless steel welds. Welding in the World. 2015; 59:239-49. https://doi.org/10.1007/s40194-014-0199-7
12. Gong W, Wang P, Zhang L, Jiang Z. Effects of Ce on microstructure and mechanical properties of LDX2101 duplex stainless steel. Metals. 2020; 10(9):1233. https://doi.org/10.3390/met10091233
13. Jiang WY, Feng YC, Wang LP, Wang JQ, Zhou PC, Guo EJ. Effect of RE content on microstructure and properties of Cr25Ni5Mo2Cu3REx duplex stainless steel. Xitu (Chinese Rare Earths). 2013; 34(2):56-60.
14. Westin EM, Olsson CO, Hertzman S. Weld oxide formation on lean duplex stainless steel. Corrosion Science. 2008; 50(9):2620-34. https://doi.org/10.1016/j.corsci.2008.06.024
15. Ouali N, Khenfer K, Belkessa B, Fajoui J, Cheniti B, Idir B, Branchu S. Effect of heat input on microstructure, residual stress, and corrosion resistance of UNS 32101 lean duplex stainless steel weld joints. Journal of Materials Engineering and Performance. 2019; 28:4252-64. https://doi.org/10.1007/s11665-019-04194-w
16. Liljas M, Johansson P, Liu HP, Olsson CO. Development of a lean duplex stainless steel. steel research international. 2008; 79(6):466-73. https://doi.org/10.1002/srin.200806154
17. Westin EM. Welds in the lean duplex stainless steel LDX 2101: effect of microstructure and weld oxides on corrosion properties (Doctoral dissertation, KTH).
18. Tseng KH, Chou CP. The effect of pulsed GTA welding on the residual stress of a stainless-steel weldment. Journal of Materials Processing Technology. 2002; 123(3):346-53. https://doi.org/10.1016/S0924-0136(02)00004-3
19. Gudikandula S, Sharma A. Study of heat input effects on the microstructure of lean Duplex 2101 shielded metal arc weld and its effect on mechanical properties, corrosion, and scratch behavior. Metallography, Microstructure, and Analysis. 2023; 12(5):834-48. https://doi.org/10.1007/s13632-023-01001-w
20. Gudikandula S, Sharma A. Microstructural behaviour and corrosion analysis of lean duplex stainless steel 2101 under the influence of variable heat inputs using gas tungsten arc welding. Iranian Journal of Materials Science and Engineering. 2022; 19(4).
21. Sharma A, Gudikandula S. The effects of heat inputs on LDSS 2101 GTAW and SMAW weld microstructure and mechanical behaviour. Archives of Metallurgy and Materials. 2024; 69(2): 685-97. https://doi.org/10.24425/amm.2024.149798
22. Verma J, Taiwade RV. Effect of welding processes and conditions on the microstructure, mechanical properties and corrosion resistance of duplex stainless-steel weldments- A review. Journal of Manufacturing Processes. 2017; 25:134-52. https://doi.org/10.1016/j.jmapro.2016.11.003
23. Muthupandi V, Srinivasan PB, Seshadri SK, Sundaresan S. Effect of weld metal chemistry and heat input on the structure and properties of duplex stainless steel welds. Materials Science and Engineering: A. 2003; 358(1-2):9-16. https://doi.org/10.1016/S0921-5093(03)00077-7
24. Kundurti SC, Sharma A. Evaluation of microstructural, mechanical and corrosion behaviours of laminated AA6061/AA7075 metal matrix composites build by friction stir additive manufacturing for structural applications. Materials Research. 2023; 26:e20230176. https://doi.org/10.1590/1980-5373-mr-2023-0176
25. Kundurti SC, Sharma A, Tambe P, Kumar A. Fabrication of surface metal matrix composites for structural applications using friction stir processing-a review.

Materials Today: Proceedings. 2022; 56:1468-77. https://doi.org/10.1016/j.matpr.2021.12.337
26. Vardhan VS, Sharma A. Investigating the degradation behaviour of grain refined WE43 magnesium alloy produced by friction stir processing for medical implant applications. Journal of Mines, Metals and Fuels. 2023; 71(12).
27. Pasha SK, Sharma A, Tambe P. Mechanical properties and tribological behaviour of Al7075 metal matrix composites: A review. Materials Today: Proceedings. 2022; 56:1513-21. https://doi.org/10.1016/j.matpr.2022.01.102
28. Harsha VS, Sharma A, Tambe P. Graphene oxide reinforced epoxy nanocomposites coatings for corrosion protection: a review. In Journal of Physics: conference series. 2022; 2225(1):12002. IOP Publishing. https://doi.org/10.1088/1742-6596/2225/1/012002
29. Prasad MD, Sharma A, Tambe P. Graphene nanoribbons reinforced polymer nanocomposites and its applications: a review. In Journal of Physics: Conference Series. 2022; 2225(1):012004. IOP Publishing. https://doi.org/10.1088/1742-6596/2225/1/012004
30. Unnikrishnan R, Idury KS, Ismail TP, Bhadauria A, Shekhawat SK, Khatirkar RK, Sapate SG. Effect of heat input on the microstructure, residual stresses and corrosion resistance of 304L austenitic stainless steel weldments. Materials Characterization. 2014; 93:10-23. https://doi.org/10.1016/j.matchar.2014.03.013
31. Kumar S, Shahi AS. Effect of heat input on the microstructure and mechanical properties of gas tungsten arc welded AISI 304 stainless steel joints. Materials and Design. 2011; 32(6):3617-23. https://doi.org/10.1016/j.matdes.2011.02.017
32. Bao LL, Wang Y, Han T. Microstructure and properties of lean duplex stainless steel UNS s32101 welded joint by hot wire tig welding. In Materials Science Forum. 2020; 993:466-73. Trans Tech Publications Ltd. https://doi.org/10.4028/www.scientific.net/MSF.993.466
33. Brytan Z, Niagaj J. Microstructural characterization of lean duplex stainless steel UNS S32101 welded joints using electron backscatter diffraction. Chiang Mai J Sci. 2013; 40(5):923-37.